INTERNATIONAL JOURNAL FOR NUMERICAL METHODS IN FLUIDS, VOL. 17, 543–566 (1993)

MULTIGRID SOLUTION OF THE NAVIER–STOKES EQUATIONS ON HIGHLY STRETCHED GRIDS

PETER M. SOCKOL

Internal Fluid Mechanics Division, NASA Lewis Research Center, Cleveland, OH 44135, U.S.A.

SUMMARY

Relaxation-based multigrid solvers for the steady incompressible Navier–Stokes equations are examined to determine their computational speed and robustness. Four relaxation methods were used as smoothers in a common tailored multigrid procedure. The resulting solvers were applied to three two-dimensional flow problems, over a range of Reynolds numbers, on both uniform and highly stretched grids. In all cases the L_2 norm of the velocity changes is reduced to 10^{-6} in a few 10's of fine-grid sweeps. The results of the study are used to draw conclusions on the strengths and weaknesses of the individual relaxation methods as well as those of the overall multigrid procedure when used as a solver on highly stretched grids.

KEY WORDS Multigrid method Navier–Stokes equations Incompressible flow

1. INTRODUCTION

In recent years there has been considerable progress in the development of multigrid solvers for the steady incompressible Navier–Stokes equations. Multigrid methods are attractive for this system because of their ability to give grid-independent convergence rates as the number of grid points is increased to large values in a fixed domain. Large numbers of points are commonly required in the solution of practical problems. The multigrid process and its application to fluid dynamics has been well described by Brandt.[1] Fuchs[2,3] examined the smoothing properties of different relaxation schemes as well as the effect of stretched grids on multigrid performance. Ghia *et al.*[4] used the streamfunction–vorticity formulation with the coupled strongly implicit scheme of Rubin and Khosla[5] as a smoothing operator and an accomodative multigrid cycle. Defect correction was used to increase the accuracy of the convection terms. Their results for the driven cavity problem are taken as the standard today. Vanka[6] employed a locally coupled Gauss–Seidel smoother for the primitive variable formulation together with an accomodative cycle. Demuren[7] extended Vanka's smoother to one in which local corrections were coupled to neighbouring pressure corrections and solved the resulting equations by both a strongly implicit technique and an alternating direction line Gauss–Seidel scheme. Thompson and Ferziger[8] used Vanka's smoother as well as a fully coupled alternating direction line Gauss–Seidel extension again with an accomodative cycle. This study also introduced defect correction together with local adaptive grid refinement. Sivaloganathan and Shaw[9] used the SIMPLE pressure-correction scheme of Patankar and Spalding[10] as a smoother for the primitive variable formulation. The smoothing analysis given in Shaw and Sivaloganathan[11] indicates that a fixed V-cycle was used in the multigrid process. Dick[12] developed a partially flux-split discretization for the primitive variable formulation and used a coupled red–black smoother and a fixed W-cycle. Finally, a few

0271–2091/93/190543–24$17.00

Received 27 October 1992
Revised 24 March 1993

solvers have used boundary-fitted curvillinear co-ordinates with primitive variables. Joshi and Vanka[13] extended Vanka's coupled Gauss–Seidel relaxation technique to this system. Rayner[14] and Shyy *et al.*[15] developed variants to the SIMPLE pressure-correction method for use as smoothers with the latter applicable to all speeds. All the last three references employed a fixed V-cycle.

In most of the above efforts, a single relaxation scheme has been used as a smoothing operator in a chosen multigrid cycle and applied to one or more problems in order to demonstrate the characteristics of the flow solver. This does not provide much guidance in the choice of smoother or multigrid cycle for the developer of a solver for a particular application. Furthermore, among the above works only Brandt,[1] Fuchs[2] and Thompson and Ferziger[8] have addressed the need for highly refined grids in local regions which is present in most flow problems. The adaptive use of several levels of uniform local subgrids[8] is attractive in the multigrid context, since it adds extra *points* only where they are needed. A more conventional approach employs stretched grids which may make it easier to resolve thin regions of steep gradients such as boundary layers adjacent to solid surfaces. This raises the question, however, as to whether fast multigrid performance can be maintained on these grids.

The present work considers the primitive variable formulation of the steady incompressible Navier–Stokes equations in Cartesian co-ordinates. Four different relaxation methods were employed as smoothers and embedded in a common tailored multigrid procedure. The resulting solvers were applied to three two-dimensional problems over a range of Reynolds numbers on both uniform and highly stretched grids. The results from this study are used to draw conclusions on the strengths and weaknesses of the individual relaxation schemes as well as those of the overall multigrid procedure when used as a solver on highly stretched grids.

2. DISCRETE FORMULATION

The steady incompressible Navier–Stokes equations in non-dimensional form are

$$\frac{\partial uu}{\partial x}+\frac{\partial uv}{\partial y}=-\frac{\partial p}{\partial x}+\frac{1}{Re}\left(\frac{\partial^2 u}{\partial x^2}+\frac{\partial^2 u}{\partial y^2}\right), \tag{1}$$

$$\frac{\partial uv}{\partial x}+\frac{\partial vv}{\partial y}=-\frac{\partial p}{\partial y}+\frac{1}{Re}\left(\frac{\partial^2 v}{\partial x^2}+\frac{\partial^2 v}{\partial y^2}\right), \tag{2}$$

$$\frac{\partial u}{\partial x}+\frac{\partial v}{\partial y}=0, \tag{3}$$

where u and v are the x and y velocity components, p is the pressure, and Re is the Reynolds number.

These equations are discretized on a staggered grid (Figure 1) using a finite volume approach

$$-R^u_{i,j}\equiv L^u u_{i,j}+\mathrm{d}y_j\Delta_x p_{i,j}=0, \tag{4}$$

$$-R^v_{i,j}\equiv L^v v_{i,j}+\mathrm{d}x_i\Delta_y p_{i,j}=0, \tag{5}$$

$$-R^c_{i,j}\equiv \mathrm{d}y_j\nabla_x u_{i,j}+\mathrm{d}x_i\nabla_y v_{i,j}=0, \tag{6}$$

where Δ_x, ∇_x, Δ_y, ∇_y, are forward and backward differences in x and y, respectively, $\mathrm{d}x_i=x_i-x_{i-1}$, $\mathrm{d}y_j=y_j-y_{j-1}$ and

$$L^u u_{i,j}=a^u_c u_{i,j}-a^u_w u_{i-1,j}-a^u_e u_{i+1,j}-a^u_s u_{i,j-1}-a^u_n u_{i,j+1}, \tag{7}$$

$$L^v v_{i,j}=a^v_c v_{i,j}-a^v_w v_{i-1,j}-a^v_e v_{i+1,j}-a^v_s v_{i,j-1}-a^v_n v_{i,j+1}. \tag{8}$$

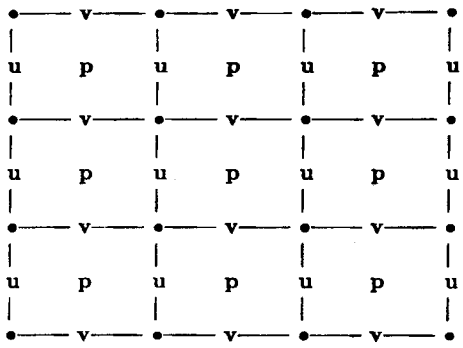

Figure 1. Variable locations on staggered grid

The coefficients a^u and a^v are defined below. When these expressions require points outside the domain, such as $L^u u_{i,j}$ adjacent to a horizontal boundary, these points are transferred to the boundary by linear extrapolation. A similar treatment is employed at an outflow boundary where $p_{i,j}$ is specified.

The coefficients in equations (7) and (8) are obtained from the hybrid scheme of Patankar and Spalding.[10] In this approximation the convective differencing in a given direction switches from second-order central to first-order upwind and the viscous term is dropped whenever the appropriate cell Reynolds number exceeds 2. The accuracy of the scheme can be improved by a defect correction technique such as that employed by Thompson and Ferziger.[8] The coefficients are first obtained for equations centred on the $p_{i,j}$ locations:

$$\begin{aligned} a_w^p &= \max(|c_w|, D_w) + c_w, \\ a_e^p &= \max(|c_e|, D_e) - c_e, \\ a_s^p &= \max(|c_s|, D_s) + c_s, \\ a_n^p &= \max(|c_n|, D_n) - c_n, \\ a_c^p &= a_w^p + a_e^p + a_s^p + a_n^p \end{aligned} \tag{9}$$

with

$$\begin{aligned} c_w &= u_{i-1,j}\,dy_j/2, \\ c_e &= u_{i,j}\,dy_j/2, \\ c_s &= v_{i,j-1}\,dx_i/2, \\ c_n &= v_{i,j}\,dx_i/2, \end{aligned} \tag{10}$$

$$\begin{aligned} D_w &= Re^{-1}\,dy_j/dx_i^a, \\ D_e &= Re^{-1}\,dy_j/dx_{i+1}^a, \\ D_s &= Re^{-1}\,dx_i/dy_j^a, \\ D_n &= Re^{-1}\,dx_i/dy_{j+1}^a \end{aligned} \tag{11}$$

and $dx_i^a = (dx_{i-1} + dx_i)/2$, $dy_j^a = (dy_{j-1} + dy_j)/2$. The coefficients a^p are stored and frozen during a sweep through the grid. The coefficients a^u and a^v are obtained by averaging. Thus,

$$(a_c^u)_{i,j} = [(a_c^p)_{i,j} + (a_c^p)_{i+1,j}]/2, \qquad (a_c^v)_{i,j} = [(a_c^p)_{i,j} + (a_c^p)_{i,j+1}]/2.$$

For the convective terms, this is equivalent to obtaining the cell face velocities by averaging. For the viscous terms, this introduces an error on a stretched grid that is of the same order as the

truncation error. In the immediate vicinity of a re-entrant corner, this practice must be modified to ensure that the convective velocity normal to the wall is set to zero.

3. RELAXATION METHODS

Each of the relaxation methods employed as a multigrid smoother in this work is adapted from, or similar to, a known technique from the literature, and hence the descriptions of the schemes will be brief. The methods are written in a common block-tridiagonal form for the corrections along a horizontal line

$$-\mathbf{A}_i\Delta\mathbf{V}_{i-1}+\mathbf{B}_i\Delta\mathbf{V}_i-\mathbf{C}_i\Delta\mathbf{V}_{i+1}=\mathbf{D}_i, \tag{12}$$

where $\Delta\mathbf{V}_i$ is the vector of local corrections, $\mathbf{A}_i$, $\mathbf{B}_i$, $\mathbf{C}_i$ are square matrices and $\mathbf{D}_i$ is the vector of local residuals. By appropriate choices of the square matrices, equation (12) can be used to describe both point or explicit schemes and semi-implicit or fully implicit schemes. This equation is now particularized for each of the methods.

The first method, here labelled Block Gauss–Seidel (BGS), is a locally coupled explicit scheme introduced by Vanka.[6] Four discrete momentum equations and one continuity equation are solved for a set of local corrections. In this case

$$\begin{aligned}\Delta\mathbf{V}_i&=(\Delta u_{i-1,j},\Delta u_{i,j},\Delta v_{i,j-1},\Delta v_{i,j},\Delta p_{i,j})^{\mathrm{T}},\\ \mathbf{D}_i&=(R^u_{i-1,j},R^u_{i,j},R^v_{i,j-1},R^v_{i,j},R^c_{i,j})^{\mathrm{T}},\end{aligned} \tag{13}$$

$\mathbf{B}_i$ is a 5×5 matrix,

$$\mathbf{B}_i=\begin{pmatrix}(a^u_c)_{i-1,j} & 0 & 0 & 0 & \mathrm{d}y_j\\ 0 & (a^u_c)_{i,j} & 0 & 0 & -\mathrm{d}y_j\\ 0 & 0 & (a^v_c)_{i,j-1} & 0 & \mathrm{d}x_i\\ 0 & 0 & 0 & (a^v_c)_{i,j} & -\mathrm{d}x_i\\ -\mathrm{d}y_j & \mathrm{d}y_j & -\mathrm{d}x_i & \mathrm{d}x_i & 0\end{pmatrix}, \tag{14}$$

and $\mathbf{A}_i=\mathbf{C}_i=\mathbf{0}$. Elimination of the Δu's and Δv's gives a simple expression for $\Delta p_{i,j}$ and back substitution then gives the local Δu's and Δv's. In a single sweep through the grid, each momentum equation is updated twice and each continuity equation once.

The second method, labelled Pressure-linked Line Block Gauss–Seidel (PLBGS), is a locally coupled semi-implicit scheme which is similar to the line relaxation scheme of Demuren.[7] This case is a simple extension of BGS:

$$\begin{aligned}\Delta\mathbf{V}_i&=(\Delta u_{i,j},\Delta v_{i,j-1},\Delta v_{i,j},\Delta p_{i,j})^{\mathrm{T}},\\ \mathbf{D}_i&=(R^u_{i,j},R^v_{i,j-1},R^v_{i,j},R^c_{i,j})^{\mathrm{T}}.\end{aligned} \tag{15}$$

$\mathbf{B}_i$ is a 4×4 matrix obtained by eliminating the top row and left column from equation (14), and $\mathbf{A}_i=\mathbf{C}_i=\mathbf{0}$ except for the lower left and upper right corner elements, respectively. Elimination of the Δu's and Δv's gives a scalar tridiagonal equation for the Δp's along the horizontal line and back substitution then gives the Δu's and Δv's along the line. During a single sweep in the $+y$-direction, each u-momentum equation is updated once, each v-momentum equation twice, and each continuity equation once. The fewer momentum updates and the efficiency of the scalar tridiagonal inversion gives a scheme that costs 15% less per sweep than BGS. In general, both x and y sweeps are combined in an alternating pattern to form an effective relaxation technique.

The third method, labelled Line Block Gauss–Seidel (LBGS), is a locally coupled, fully implicit scheme, which is apparently very similar to the coupled alternating line approach of Thompson and Ferziger.[8] The vectors $\Delta\mathbf{V}_i$ and $\mathbf{D}_i$ and the matrix $\mathbf{B}_i$ are the same as for PLBGS, while $\mathbf{A}_i$ and $\mathbf{C}_i$ are 4×4 matrices having diagonal plus the lower left and upper right corner elements, respectively. The number of equation updates and sweeping patterns are the same as for PLBGS. In this case algebraic elimination in the block-tridiagonal inversion gives a scheme that costs only 15% more per sweep than BGS.

The final method is the Semi-Implicit Pressure-Correction scheme (SIMPLE) introduced by Patankar and Spalding.[10] In this case

$$\begin{aligned}\Delta\mathbf{V}_i&=(\Delta u_{i,j},\Delta v_{i,j})^{\mathrm{T}},\\ \mathbf{D}_i&=(R^u_{i,j},R^v_{i,j})^{\mathrm{T}},\end{aligned}\tag{16}$$

where $\mathbf{A}_i$, $\mathbf{B}_i$, $\mathbf{C}_i$ are diagonal 2×2 matrices. The pressure is obtained from an elliptic equation derived by substituting reduced forms of the discrete momentum equations for coupled velocity and pressure corrections into continuity. For this work one SIMPLE iteration consists of a single scalar line Gauss–Seidel sweep for each momentum equation with the pressure fixed. This is followed by four alternating direction line Gauss–Seidel sweeps of the elliptic pressure-correction equation. Taking more than one sweep through the momentum equations before correcting the pressure *invariably* resulted in partial decoupling of the velocity components and slower convergence. Each of these combined SIMPLE iterations costs about 30% more than one sweep of BGS.

For each of these relaxation techniques, some degree of underrelaxation is required to obtain convergence. In the present work this is implemented through direct modification of the momentum equations. For BGS, LBGS and SIMPLE, the diagonal velocity coefficients, a^u_c and a^v_c, in the matrix $\mathbf{B}_i$ are divided by a factor r_{mom}, where $0<r_{\mathrm{mom}}<1$. For PLBGS the residuals, R^u and R^v, are multiplied by r_{mom}. In addition, for SIMPLE the pressure corrections and the corresponding velocity corrections required to satisfy continuity are unrelaxed.

Finally, we note that considerable improvement can be obtained with each of the above methods by employing a symmetric sweeping pattern. Thus, for BGS each lexicographic sweep is followed by one in the reverse direction. For PLBGS, LBGS and SIMPLE, a four sweep symmetric alternating line pattern is used, i.e. relaxation is performed sequentially in the $+x$, $+y$, $-y$ and $-x$ directions. These techniques result in an approximately 25% improvement in convergence rates.

4. MULTIGRID ITERATION

Local relaxation methods, such as those of the previous section, are in general much more efficient at reducing short-wavelength error components on a given grid than those of longer wavelength. Multigrid seeks to overcome this problem by transferring the long-wave components of the solution to a sequence of coarser grids where relaxation is more effective and much cheaper. Since the FAS–FMG (full approximation scheme–full multigrid) technique used in this work has been well documented in the literature,[1,4,6–9] the present description of the multigrid process will be brief. The focus will, instead, be on the current implementation and in particular on those aspects which are important in achieving a fast robust Navier–Stokes solver.

Introduce a sequence of grids k, where $k=1$ is the coarsest and $k=m$ is the finest grid. On any grid the system of equations is represented by

$$L^kU^k=F^k,\tag{17}$$

where L^k is a discrete approximation to the differential operator on grid k, U^k is the vector of unknowns and F^k is defined below. Next define a relaxation operator S^k for equation (17), a fine-to-coarse grid restriction operator $\hat{I}_{k+1}^k$ for unknowns, a restriction operator I_{k+1}^k for residuals, $R^k = F^k - L^k U^k$, and a coarse-to-fine grid prolongation operator for corrections I_k^{k+1}. With these definitions, the FAS multigrid cycle M^k for improving an approximation U^k is defined recursively as follows:

If $k=m$, F^k is the right-hand side of the discrete system.
If $k=1$, solve equation (17) by several relaxation sweeps.
If $k>1$, do these six steps:

(a) Relax on grid k,

$$U^k \leftarrow (S^k)^{\nu_1} U^k.$$

(b) Restrict U^k to grid $k-1$,

$$U^{k-1} \leftarrow \hat{I}_k^{k-1} U^k.$$

(c) Restrict R^k to grid $k-1$ and form source term

$$F^{k-1} \leftarrow L^{k-1} U^{k-1} + I_k^{k-1} R^k. \tag{18}$$

(d) Perform γ multigrid cycles on U^{k-1}:

$$U^{k-1} \leftarrow (M^{k-1})^{\gamma} U^{k-1}.$$

(e) Prolong corrections to grid k,

$$U^k \leftarrow U^k + I_{k-1}^k (U^{k-1} - \hat{I}_k^{k-1} U^k).$$

(f) Relax on grid k,

$$U^k \leftarrow (S^k)^{\nu_2} U^k.$$

For $\gamma=1$, this is called a V-cycle or $V(\nu_1, \nu_2)$, and for $\gamma=2$, this is called a W-cycle or $W(\nu_1, \nu_2)$. Finally, the full FAS–FMG technique is obtained by starting the computation on a very coarse grid, iterating to 'convergence' with the FAS process, and interpolating the result to obtain the initial values on the next finest grid. In this way the first approximation on the finest grid is already close in much of the domain, an important consideration in non-linear problems. Convergence criteria for each stage in the FAS–FMG process as used in the present work are explained in Section 5.

In the present work the coarse grids are created by 'standard coarsening', i.e. every second grid point in both x and y is deleted from one grid to the next coarser grid. The fine-to-coarse restriction operator $\hat{I}_f^c$ employs cell-face averaging for the velocities,

$$u_{i,j}^c = (u_{i,j-1}\,\mathrm{d}y_{j-1} + u_{i,j}\,\mathrm{d}y_j)/\mathrm{d}y_j^c, \qquad v_{i,j}^c = (v_{i-1,j}\,\mathrm{d}x_{i-1} + v_{i,j}\,\mathrm{d}x_i)/\mathrm{d}x_i^c, \tag{19}$$

and full weighting for the pressures,

$$p_{i,j}^c = (p_{i-1,j-1}\,\mathrm{d}x_{i-1}\,\mathrm{d}y_{j-1} + p_{i-1,j}\,\mathrm{d}x_{i-1}\,\mathrm{d}y_j + p_{i,j-1}\,\mathrm{d}x_i\,\mathrm{d}y_{j-1} + p_{i,j}\,\mathrm{d}x_i\,\mathrm{d}y_j)/(\mathrm{d}x_i^c\,\mathrm{d}y_j^c), \tag{20}$$

where $(\,)^c$ represents a coarse-grid value. The restriction operator I_f^c for residuals uses full weighting, in which all the fine-grid contributions to a coarse-grid cell are accounted for (Figure 2):

$$\begin{aligned}(I_f^c R^u)_{i,j} &= R_{i,j-1}^u + R_{i,j}^u + \tfrac{1}{2}(R_{i-1,j-1}^u + R_{i-1,j}^u + R_{i+1,j-1}^u + R_{i+1,j}^u),\\ (I_f^c R^v)_{i,j} &= R_{i-1,j}^v + R_{i,j}^v + \tfrac{1}{2}(R_{i-1,j-1}^v + R_{i,j-1}^v + R_{i-1,j+1}^v + R_{i,j+1}^u),\end{aligned} \tag{21}$$

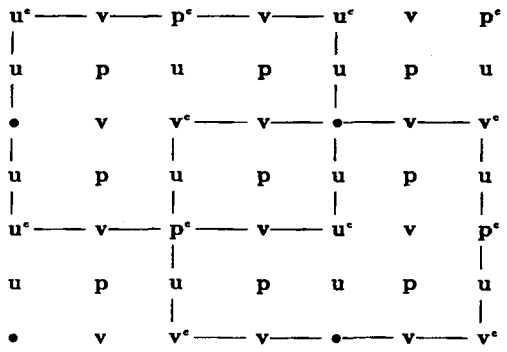

Figure 2. Variable locations on fine and coarse staggered grids showing control volumes for full weighting of residuals

where R^u and R^v, given by equation (4) and (5), are already area-weighted. With the cell-face averaging given by equation (19) and full weighting similar to equation (20) for R^c, as defined by equation (6), the coarse-grid source term of equation (18) vanishes for the continuity equation.

In many of the previous works[6, 7, 9, 15] cell-face averaging was also used in the restriction of R^u and R^v. For uniform grids this has little effect on the multigrid convergence rate. For the highly stretched grids employed in this work, this proved to be ineffective. In some cases convergence slowed by a factor of 3 or 4. In others, little or no benefit was gained from the multigrid process.

The coarse-to-fine prolongation operator I_c^f for corrections employs bilinear interpolation in computational space where the grid spacing is taken to be uniform. For fine grid points adjacent to boundaries, zero normal gradient is assumed for pressures. The overall convergence has proven to be insensitive to the details of this approximation. The same operator with one modification is also used to interpolate 'converged' results to obtain initial values on a fine grid in the FMG process. The velocity component parallel to an adjacent wall is obtained by bilinear extrapolation from the interior, since the boundary layer is poorly resolved on the coarse grid.

The multigrid solvers in this work have been coded to permit fixed V and W-cycles. During the course of this effort it was found that for the difficult cases with high Reynolds numbers or highly stretched grids a $W(1, 1)$ cycle was the most effective strategy in terms of robustness and computational cost. Hence, all results presented in this paper were performed using this cycle. Accomodative cycles,[1, 4, 6–8] which decide on whether or not to restrict to a coarser grid based on the ratio of errors from two successive sweeps, proved to be too costly, since the second sweep on each visit to a grid contributed little to the overall convergence of the method.

The symmetric sweeping pattern described in Section 3 has been interleaved with the multigrid process. A sweep counter is established for every grid level and on each visit to that level the next direction in the sweep pattern for that grid is performed. This proved to be sufficient to give all the convergence benefits of the sweeping symmetry. Finally, it should be noted that varying the momentum relaxation factor r_{mom} from grid to grid during the cycle provided considerable performance enhancement for the BGS, PLBGS and LBGS solvers. However, no benefit was observed when this was tried with the SIMPLE-based solver.

5. CONVERGENCE CRITERIA

The various convergence criteria used in this work are all based on an L_2 norm of the dynamic velocity changes occurring during a sweep through the grid. This would seem to be a more

appropriate form for a system of coupled equations than one based on a combination of the residuals of the different equations. The pressures have been excluded, since they are only determined to within an arbitrary constant. Introduce the definition

$$\varepsilon^k = \sqrt{\left\{ \sum_{i,j=1}^{n_x^k, n_y^k} [(\Delta u_{i,j}^k)^2 + (\Delta v_{i,j}^k)^2]/(2n_x^k n_y^k) \right\}}, \tag{22}$$

where n_x^k and n_y^k are the number of cells on grid k in x and y, respectively, and $\Delta u_{i,j}^k$, $\Delta v_{i,j}^k$ are the dynamic velocity changes obtained during a sweep on grid k. Then for a sequence of coarse-to-fine grids, $k=1$ to m, the overall convergence criterion on grid m is taken as

$$\varepsilon^m < 10^{-6}. \tag{23}$$

In most cases at convergence given by equation (23) the value of $\max(\Delta u, \Delta v)$ is approximately 10^{-5}. For intermediate grids in the FAS–FMG process, convergence before interpolating to the next finer grid is taken as

$$\varepsilon^k < 10^{-3}, \tag{24}$$

and for the coarsest grid, $k=1$, 'solution' is given by

$$\varepsilon^1 < \varepsilon^k/10, \tag{25}$$

where now ε^k is the most recent error on the current finest grid.

Finally, it is noted that all computations in this work were performed on an Amdahl 5980 in scalar mode. All cpu times reported in the next sections are for this machine.

6. COMPUTATIONAL RESULTS

Three problems have been chosen to test the performance of the multigrid solvers under different conditions: flow in a driven cavity, developing flow in a straight channel, and flow over an open cavity.

6.1. Driven cavity flow

The driven cavity is the prototypical recirculating flow and has long been used as a standard test problem for Navier–Stokes solvers. The second-order streamfunction–vorticity results of Ghia *et al.*[4] are generally accepted as the standard. Flow is set up in a square cavity with three stationary walls and a top lid that moves to the right with constant speed ($u=1$). Streamfunction contours for $Re=1000$ and 5000 are shown in Figure 3, and u-velocities on the vertical centreline computed on a uniform 256×256 grid for the same Reynolds numbers are compared with the standard results[4] in Figure 4. At $Re=1000$, the two computations agree within plotting accuracy. At $Re=5000$, the discrepancy is a result of the excessive dissipation of the hybrid differencing scheme.

The first set of results for this flow is for a uniform grid with Re varying from 100 to 5000. Convergence plots of the L_2 norm of the velocity changes ($L_2 \Delta V$) vs. work units are shown in Figure 5 for all methods on a 256×256 grid where a work unit is the cpu time required for one fine-grid sweep of the particular smoother. In this figure each symbol on a plot represents a single fine-grid sweep and the horizontal offset from the origin is the initialization time on the coarser grids. These plots give an indication of multigrid performance that is independent of the differences in cpu time per sweep for each solver. On this basis all of the solvers are competitive but BGS and PLBGS show a small advantage. Table I compares the uniform-grid results for each

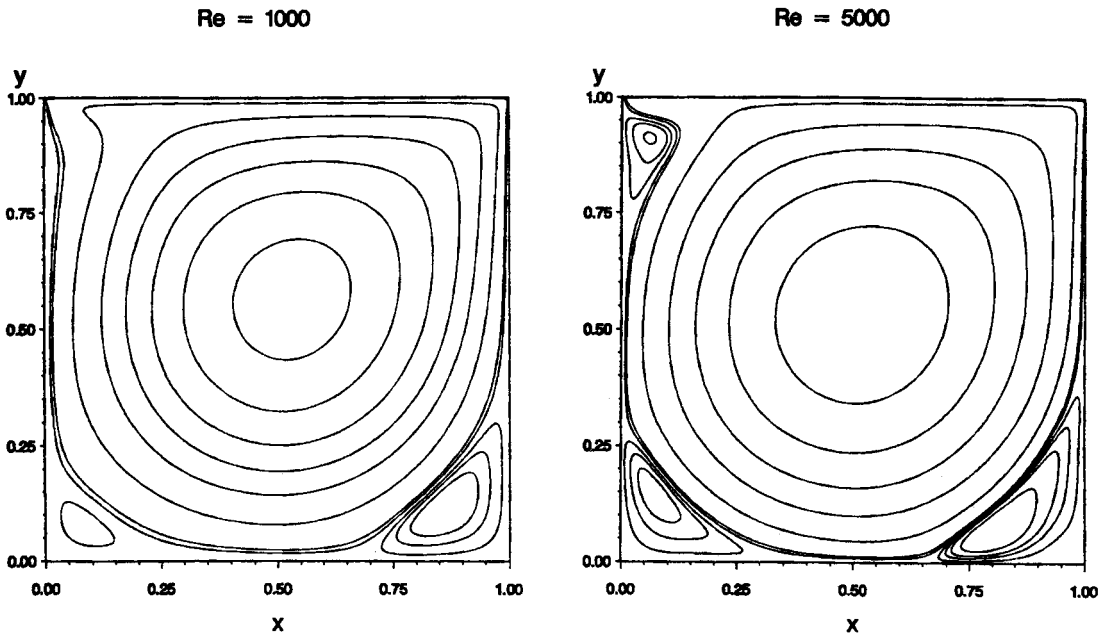

Figure 3. Driven cavity stream function contours for $Re = 1000$ and 5000

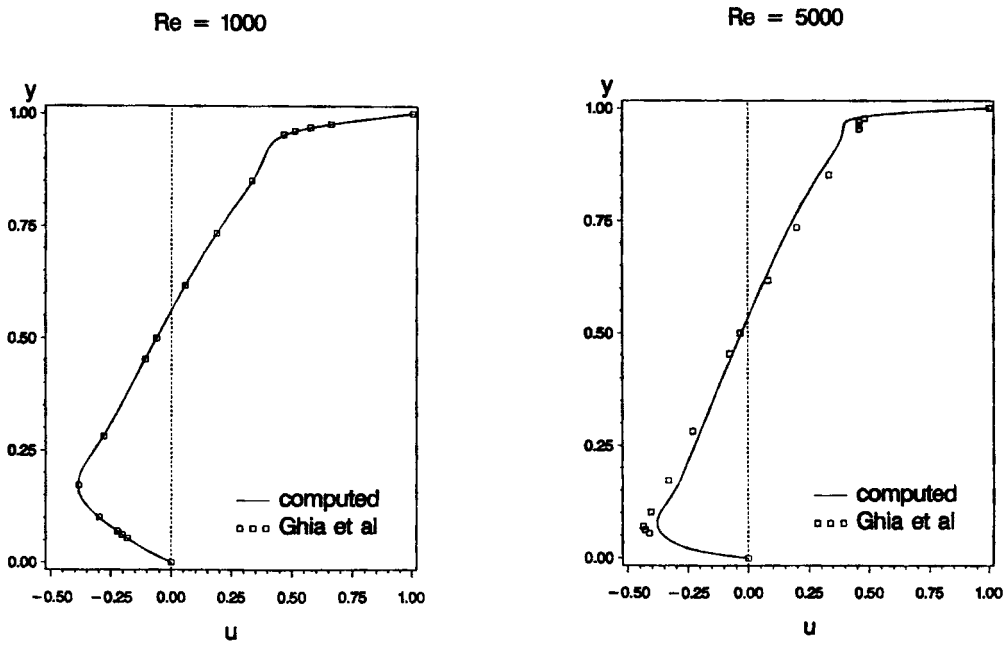

Figure 4. Driven cavity u-velocities on vertical centreline computed on a uniform 256×256 grid for $Re = 1000$ and 5000

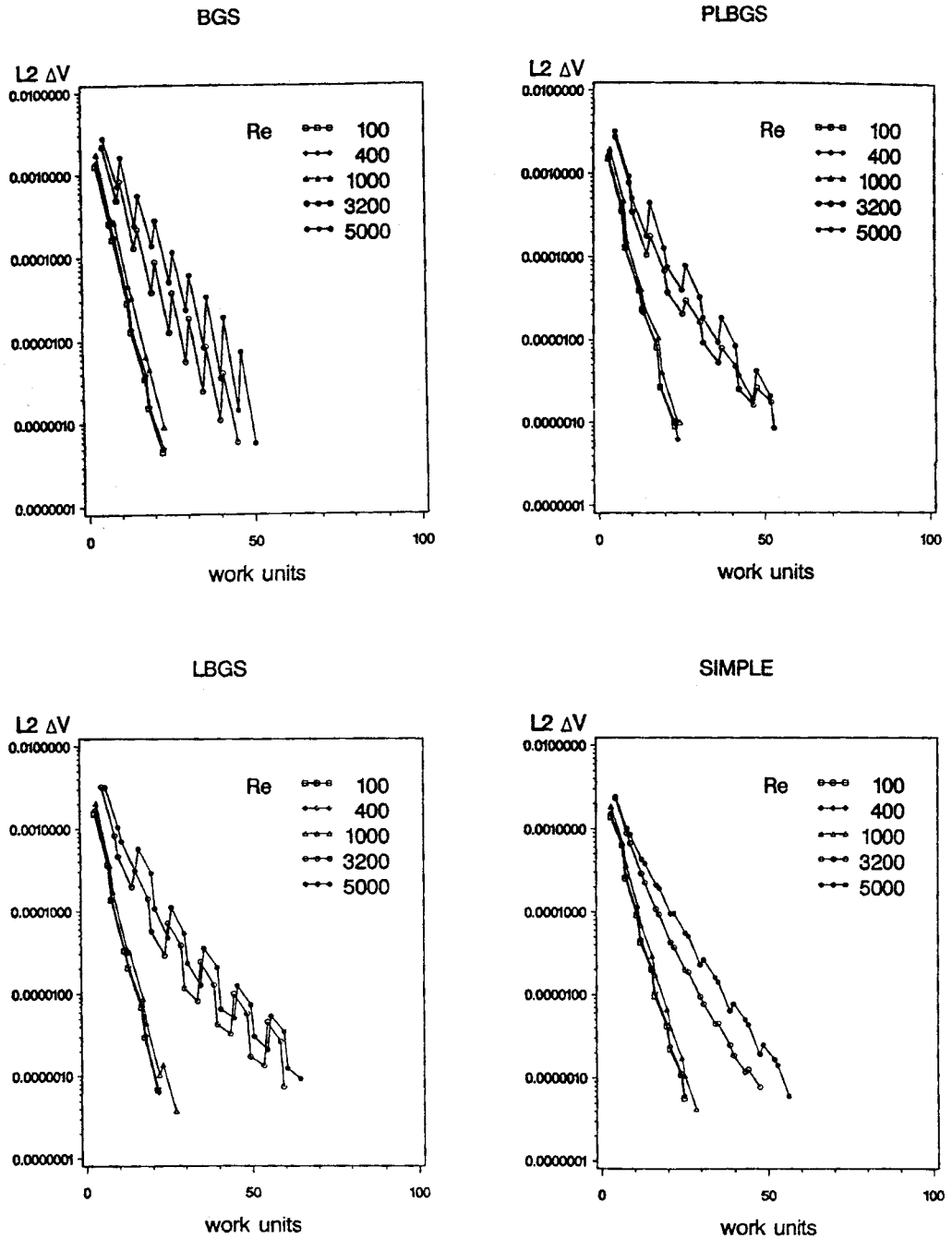

Figure 5. Driven cavity convergence histories for all methods on a uniform 256 × 256 grid

Table I. Driven cavity convergence on uniform grids for AR = 1

Scheme (r^{fg}_{mom})	*Re*				
	100	400	1000	3200	5000
	(cpu seconds/fine-grid sweeps/work units)				
	128 × 128 grid—6 levels				
BGS (0·7)	31·9	35·5	49·0	73·7	104·1
	8	9	12	18	26
	22·5	25·0	34·5	51·4	73·0
PLBGS (0·8)	34·8	35·4	51·0	78·8	97·7
	10	10	15	23	28
	28·8	29·0	42·1	64·6	80·0
LBGS (0·8)	36·8	45·4	69·8	105·6	115·8
	9	10	16	24	27
	22·6	28·1	43·2	65·0	71·4
SIMPLE (0·7)	58·0	58·9	77·5	134·0	179·2
	12	12	16	28	38
	31·6	31·9	42·2	72·8	97·1
	256 × 256 grid — 7 levels				
BGS (0·7)	128·0	130·5	131·2	259·4	294·1
	8	8	8	16	18
	22·2	22·6	22·7	44·9	50·2
PLBGS (0·8)	114·0	119·7	123·9	262·2	263·1
	8	9	9	19	19
	22·9	23·9	24·6	52·9	52·7
LBGS (0·3)	141·9	144·5	178·6	389·7	423·8
	8	8	10	23	24
	21·4	21·7	27·0	59·3	64·4
SIMPLE (0·7)	217·1	218·6	250·1	414·6	491·4
	11	11	12	20	24
	24·9	25·1	28·6	47·5	56·3

solver on two grids in terms of cpu times, number of fine-grid sweeps and total work units for each case. Here r^{fg}_{mom} is the fine-grid relaxation factor for the solver. As the Reynolds number increases and the grid is made finer, the table indicates a significant advantage for BGS and PLBGS over LBGS and SIMPLE due to faster convergence and less cost per sweep. Also note that fewer sweeps are needed on the finer grid for all methods.

The second set of results is obtained for $Re = 1000$ on a grid with hyperbolic tangent stretching in x and y and the maximum mesh aspect ratio (AR) varying from 1 to 40. The grid for AR = 10 is shown in Figure 6. Convergence plots for all methods on a 256 × 256 grid are shown in Figure 7. For this case it is seen that BGS and SIMPLE show substantially better multigrid performance than the other two solvers. Table II compares the stretched-grid results for each solver on two grid sizes. As AR is increased to large values and the number of grid points is increased, BGS is seen to have a significant advantage over the other three methods in both number of sweeps and cpu time. The use of highly stretched grids produces a strong asymmetry in the momentum

Table II. Driven cavity convergence on stretched grids for $Re = 1000$

Scheme (r^{fg}_{mom})	AR				
	1	5	10	20	40
	(cu seconds/fine-grid sweeps/work units)				
			128 × 128 grid — 6 levels		
BGS (0·6)	55·8	56·6	64·1	77·0	84·3
	14	14	16	20	22
	39·6	39·7	44·7	54·0	59·3
PLBGS (0·5)	63·6	55·6	63·3	76·3	77·1
	19	16	19	23	23
	52·5	45·5	51·7	62·6	62·6
LBGS (0·9)	79·4	95·1	94·7	101·5	111·5
	19	23	23	24	27
	48·9	57·7	57·6	61·5	67·4
SIMPLE (0·7)	78·5	80·6	80·10	89·3	96·1
	16	17	17	18	20
	42·1	42·7	42·8	46·6	51·4
			256 × 256 grid — 7 levels		
BGS (0·6)	160·1	162·2	163·1	193·2	191·3
	10	10	10	12	12
	27·8	27·9	27·9	32·8	32·9
PLBGS (0·5)	171·1	171·3	198·6	251·1	284·9
	12	12	14	18	21
	34·2	33·9	39·3	49·9	56·3
LBGS (0·9)	145·9	185·4	252·2	352·8	490·9
	8	11	15	21	29
	22·0	27·5	37·4	52·2	72·2
SIMPLE (0·7)	248·2	221·0	222·0	251·4	290·8
	12	11	11	12	14
	28·5	25·3	25·3	28·5	33·1

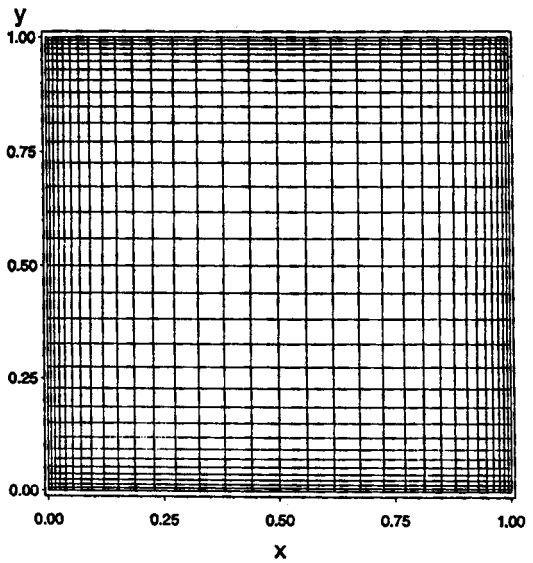

Figure 6. Driven cavity stretched grid with AR = 10

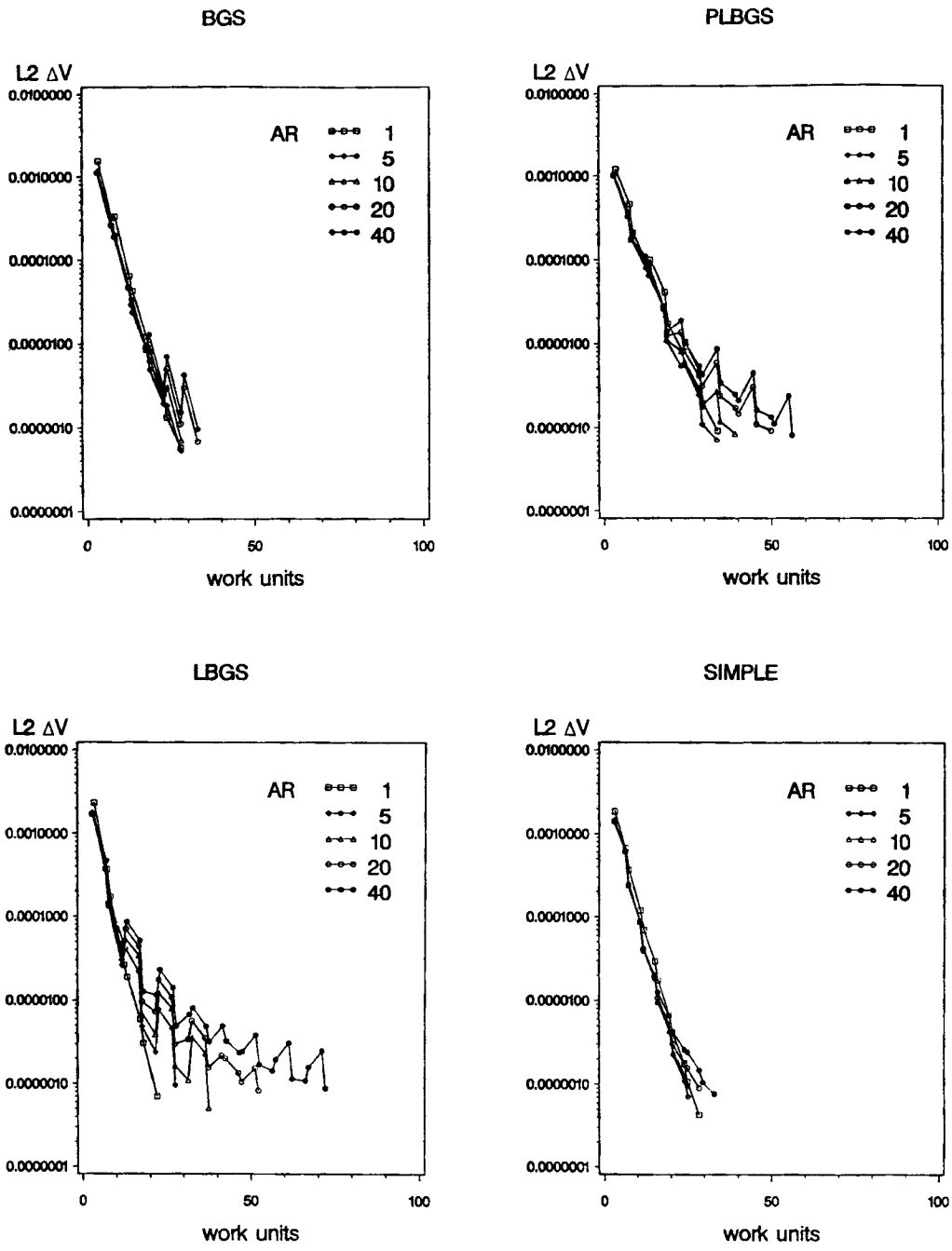

Figure 7. Driven cavity convergence histories for all methods on a stretched 256 × 256 grid

equation coupling coefficients [equations (9)] in regions of high mesh aspect ratio and this was expected to adversely affect the smoothing properties of an explicit scheme[1] such as BGS. The alternating direction semi-implicit and fully implicit schemes were introduced to see if they would give more robust performance for these cases. This proved not to be true for the Navier–Stokes solvers used in this study.

6.2. Developing channel flow

The second test problem is the deceptively simple one of developing flow in a straight channel one unit high and four units long. Uniform velocities ($u=1, v=0$) are specified at the entrance and a constant pressure ($p=0$) is set at the exit. Note, for incompressible flow, the common exit condition, $\partial u/\partial x=0$, implies $\partial v/\partial y=\partial p/\partial y=0$. Profiles of u vs. y along the channel for $Re=1000$ and 5000 are shown in Figure 8. For these Reynolds numbers, the flow is far from fully developed at the exit. This flow has velocities strongly aligned with the x-direction over much of the domain and the u-momentum equation becomes increasingly decoupled in y away from the walls as Re is increased. This situation is known to cause problems for multigrid solvers (see e.g. References 1 and 16) and, thus, was chosen as a fitting test case for this study.

The first set of results is for a uniform grid with Re again varying from 100 to 5000. Convergence plots of $L_2\Delta V$ vs. work units for all methods on a 256×64 grid are shown in Figure 9. It is evident that the multigrid performance of all the solvers degrades more rapidly with increasing Re than was the case for the driven cavity with SIMPLE falling off much more than the others. The uniform-grid results for each solver on two grids are compared in Table III and confirm those shown by Figure 9 when both fine-grid sweeps and cpu time are considered. The

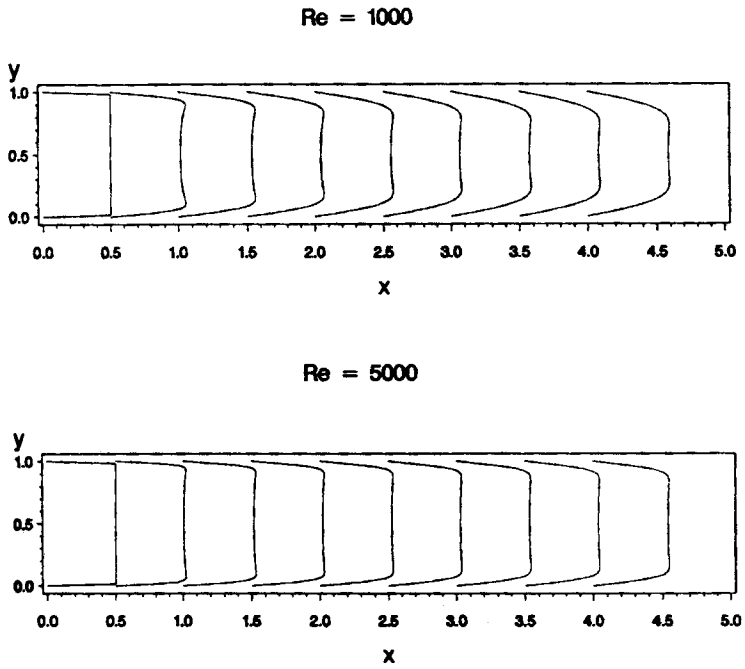

Figure 8. Developing channel u-velocity profiles for $Re=1000$ and 5000

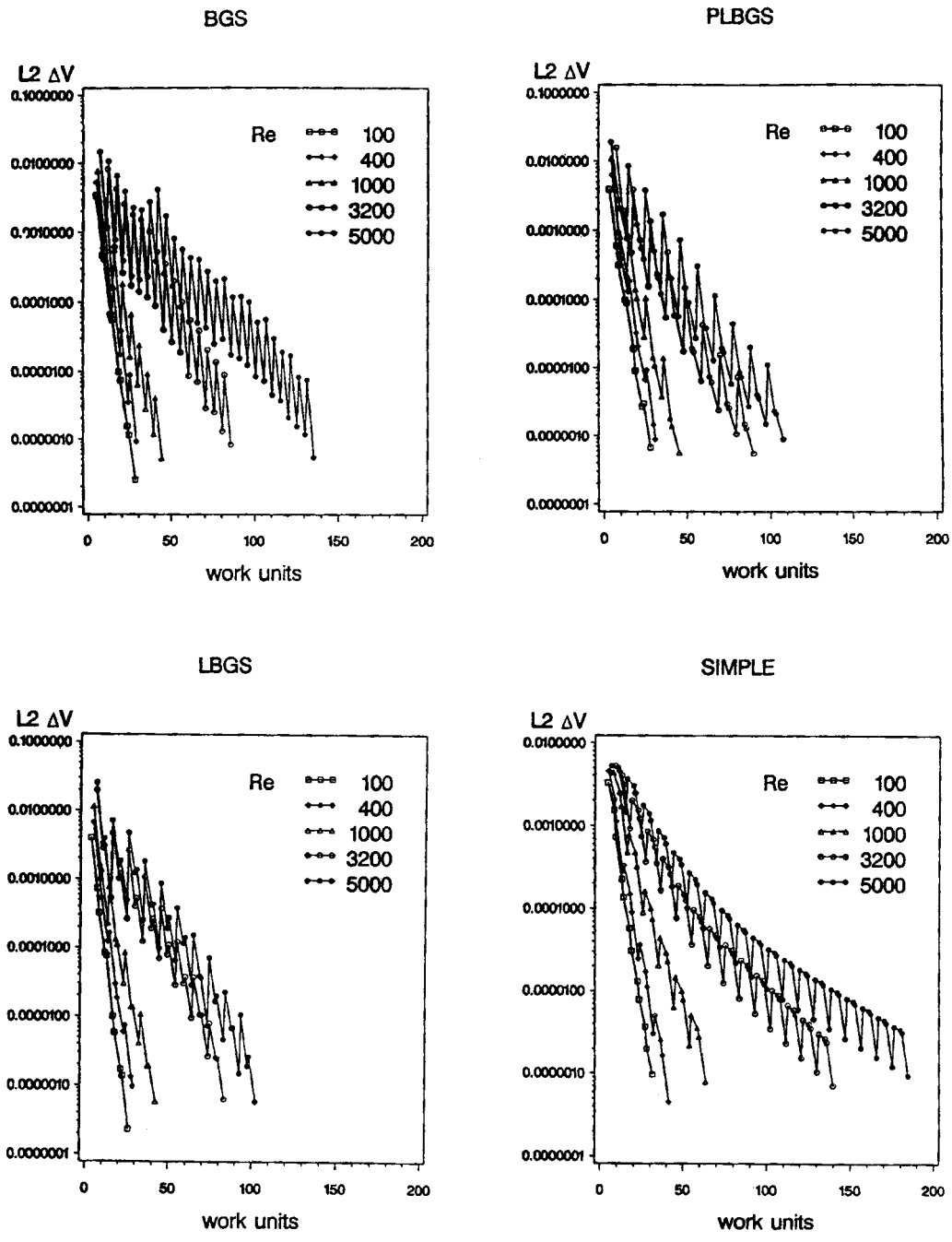

Figure 9. Developing channel convergence histories for all methods on a uniform 256 × 64 grid

Table III. Developing channel convergence on uniform grids for AR = 1

Scheme (r^{fg}_{mom})	*Re* 100	400	1000	3200	5000
	(cpu seconds/fine-grid sweeps/work units)				
			128 × 32 grid—4 levels		
BGS (0·7)	10·3	16·5	24·4	46·3	53·1
	10	16	24	48	58
	27·2	43·5	64·8	122·2	140·4
PLBGS (0·8)	9·5	15·1	24·4	41·0	50·2
	11	16	28	48	60
	29·8	47·2	75·4	126·9	155·7
LBGS (0·8)	11·4	18·2	26·2	32·9	41·3
	10	16	24	32	40
	27·1	43·0	61·6	78·2	97·0
SIMPLE (0·7)	16·9	28·7	50·5	84·9	93·4
	14	24	44	80	88
	36·1	60·9	107·5	181·7	198·4
			256 × 64 grid — 5 levels		
BGS (0·7)	42·5	44·0	66·6	129·1	206·4
	10	10	16	32	52
	28·0	28·5	44·2	85·4	135·4
PLBGS (0·8)	36·9	40·8	59·7	118·2	141·7
	10	11	16	32	40
	28·1	30·9	45·4	89·9	108·0
LBGS (0·8)	45·3	49·9	73·2	144·1	177·7
	10	11	16	32	40
	26·3	28·9	42·4	83·3	102·3
SIMPLE (0·7)	60·0	79·3	120·5	264·1	350·0
	12	16	24	56	76
	31·7	41·6	63·6	139·9	184·5

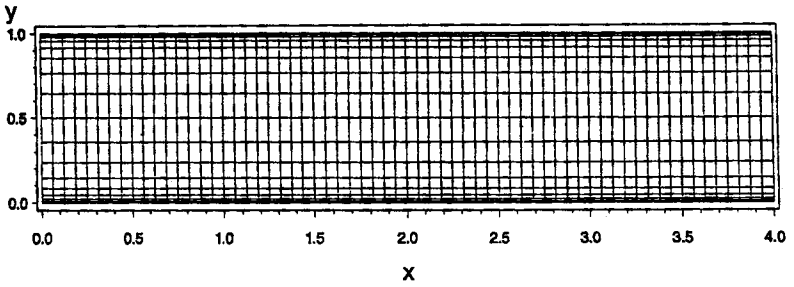

Figure 10. Developing channel stretched grid with AR = 10

relatively poor performance of SIMPLE is probably due to the partial decoupling between u and v at high Re which was observed during the iterative process. However, note that all methods still converged in under 100 fine-grid sweeps even at the highest Reynolds numbers.

The second set of results for this flow is for hyperbolic tangent stretching in y only, again with AR varying from 1 to 40 and $Re = 1000$. The grid for AR = 10 is shown in Figure 10. Convergence plots for all methods on a 256×64 grid are shown in Figure 11. Here it is obvious that LBGS shows markedly better multigrid performance than the other methods. Stretched-grid results for each solver on two grid sizes are compared in Table IV. As AR is increased to large values for each grid size, it is evident that LBGS has a major advantage over the other smoothers in both fine-grid sweeps and cpu time. This case of strong alignment on a stretched grid is the only one in which an implicit scheme (LBGS) has a substantial advantage over the explicit BGS.

Table IV. Developing channel convergence on stretched grids for $Re = 1000$

Scheme (r^{fg}_{mom})	AR				
	1	5	10	20	40
	(cpu seconds/fine-grid sweeps/work units)				
	128×32 grid—4 levels				
BGS (0·7)	24·6	50·6	55·4	48·7	41·9
	24	54	58	50	42
	64·6	131·3	144·2	126·4	108·5
PLBGS (0·7)	31·0	34·0	41·0	44·9	55·3
	36	40	48	52	64
	96·0	103·2	125·5	137·9	170·4
LBGS (0·85)	30·1	21·8	21·8	22·0	23·1
	28	20	20	20	20
	71·0	50·4	50·8	51·1	53·4
SIMPLE (0·7)	50·4	49·1	62·3	70·7	70·7
	44	44	56	64	64
	107·2	103·7	130·8	148·9	148·8
	256×64 grid—5 levels				
BGS (0·7)	66·9	89·6	122·6	198·8	177·1
	16	22	30	50	44
	44·2	58·3	78·7	128·8	113·9
PLBGS (0·7)	73·7	72·3	95·5	114·4	167·3
	20	20	27	32	47
	55·7	53·8	71·0	85·7	125·4
LBGS (0·85)	73·3	46·8	64·2	65·7	75·5
	16	10	14	14	16
	42·4	26·7	36·3	37·4	42·7
SIMPLE (0·7)	119·9	97·8	114·5	134·4	209·2
	24	20	24	28	44
	63·6	50·8	59·6	70·0	107·7

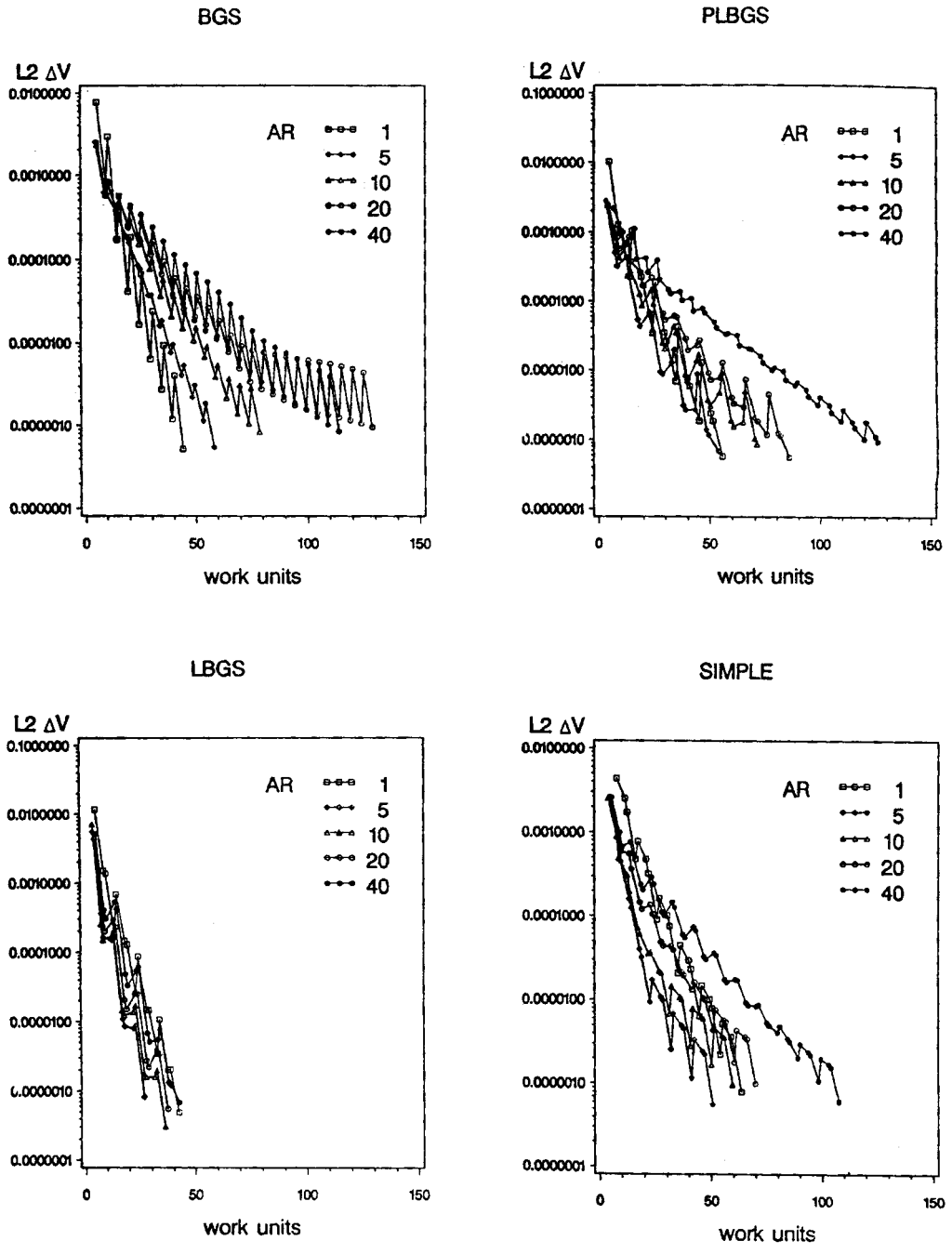

Figure 11. Developing channel convergence histories for all methods on a stretched 256 × 64 grid

6.3. *Open cavity flow*

The final test problem combines the driven cavity and developing channel flows and adds the complication of a strong corner singularity. The domain consists of a channel one unit high and two units long on the top of an open cavity one unit square located at the left boundary. Uniform flow ($u=1$, $v=0$) enters the channel at the left and exits at the right ($p=0$). Streamfunction and vorticity contours for $Re=1000$ are shown in Figure 12. Note the lack of separation and the strong concentration of vorticity contours at the downstream corner.

As before the first set of results is for a uniform grid with Re varying from 100 to 5000. Convergence plots of $L_2\Delta V$ vs. work units for all methods on a $128\times128+256\times128$ grid are shown in Figure 13. As was the case with the channel flow the multigrid performance of SIMPLE is seen to degrade more rapidly than that of the other methods as Re is increased. The uniform-grid results for each solver on two grids are compared in Table V. The results for fine-grid sweeps and cpu time confirm that BGS, PLBGS and LBGS remain competitive as Reynolds number is increased but SIMPLE suffers a substantial penalty.

The second set of results for this flow is for hyperbolic tangent stretching in both x and y, in each of three square regions, with AR varying from 1 to 40 and $Re=1000$. The grid for AR = 10 is shown in Figure 14. Convergence plots for all methods on a $128\times128+256\times128$ grid are shown in Figure 15. In this case, BGS shows a small advantage over the other methods in multigrid performance. The stretched-grid results for each solver on two grid sizes are compared in Table VI. Here it is evident that BGS has a significant advantage in fine-grid sweeps and cpu time as AR increases. It should also be noted that PLBGS and LBGS appeared to be more sensitive to the presence of the corner singularity and to the choice of r_{mom} for the set of grids used in the multigrid process. However, no detailed study of this effect was performed.

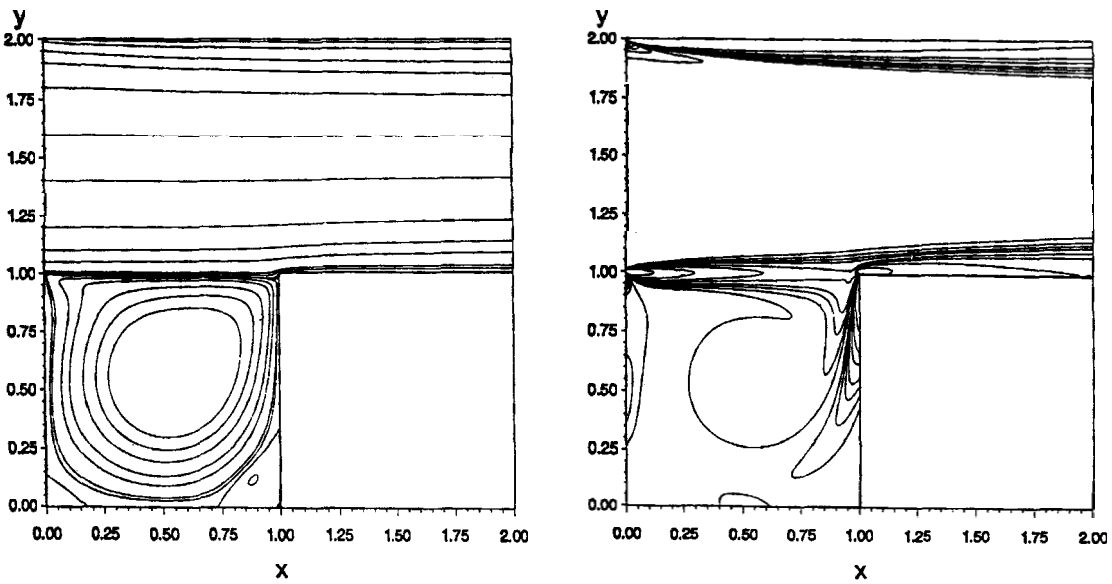

Figure 12. Open cavity stream function (left) and vorticity (right) contours for $Re=1000$

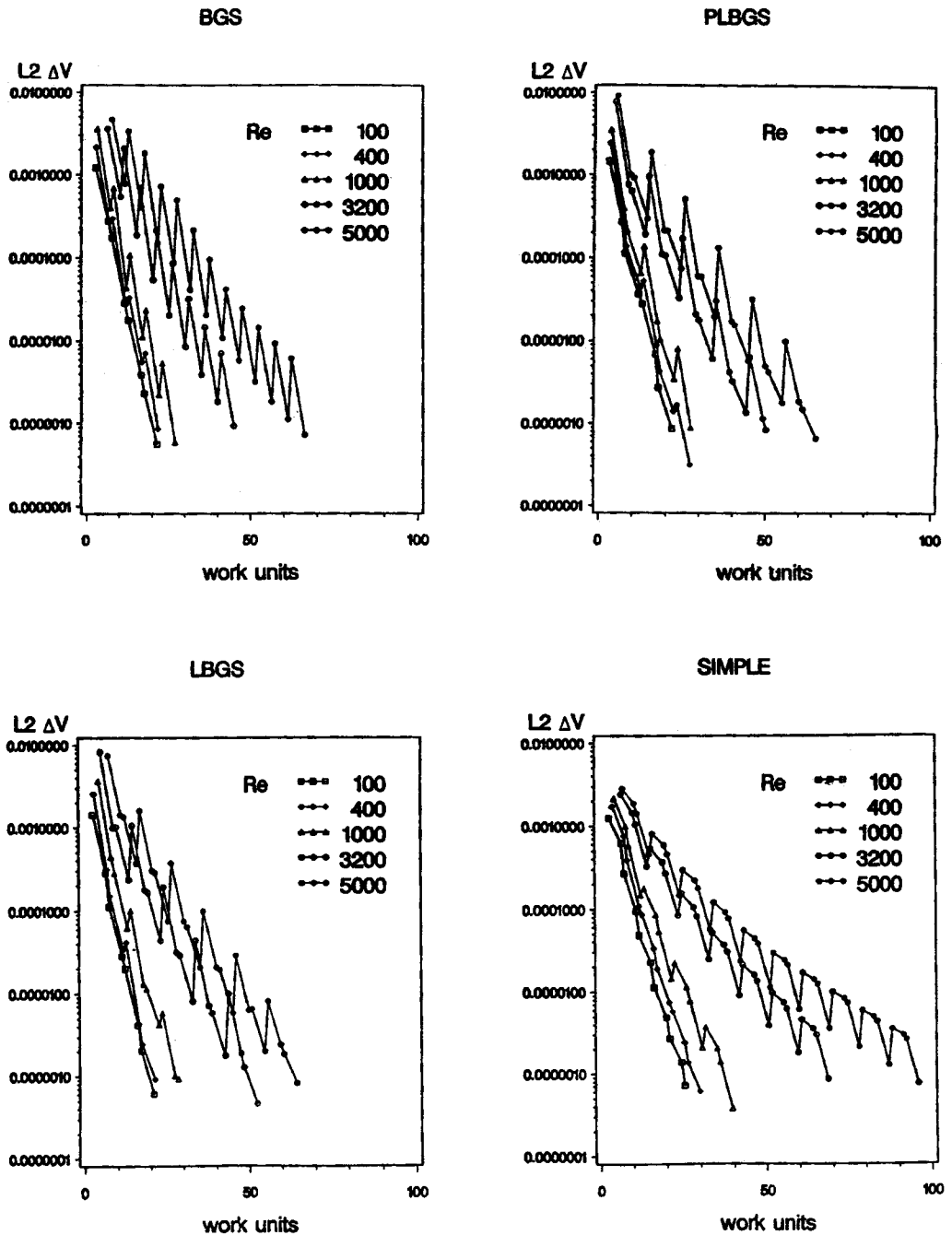

Figure 13. Open cavity convergence histories for all methods on a uniform $128 \times 128 + 256 \times 128$ grid

Table V. Open cavity convergence on uniform grids for AR = 1

Scheme (r^{fg}_{mom})	Re				
	100	400	1000	3200	5000
	(cpu seconds/fine-grid sweeps/work units)				
	$64 \times 64 + 128 \times 64$ grid — 5 levels				
BGS (0·7)	34·2	35·4	48·8	108·1	134·9
	10	10	14	32	40
	28·1	29·0	40·3	88·5	110·0
PLBGS (0·8)	29·7	32·9	48·3	92·6	118·1
	10	11	16	32	40
	28·7	31·6	46·4	89·6	113·5
LBGS (0·8)	35·8	45·3	59·3	101·3	124·1
	10	12	16	28	35
	26·5	33·4	43·9	75·6	92·5
SIMPLE (0·7)	47·6	62·6	95·1	193·7	253·8
	12	16	24	52	68
	31·2	41·7	62·9	127·9	167·0
	$128 \times 128 + 256 \times 128$ grid — 6 levels				
BGS (0·7)	115·9	116·7	144·2	241·2	355·9
	8	8	10	16	24
	21·6	21·8	27·1	44·9	66·4
PLBGS (0·8)	102·5	127·9	129·1	233·4	304·7
	8	10	10	19	24
	22·0	27·5	27·7	50·3	65·4
LBGS (0·8)	123·1	125·9	167·4	305·4	377·9
	8	8	11	20	24
	21·0	21·3	28·5	52·4	64·6
SIMPLE (0·7)	179·7	209·8	279·7	486·2	681·4
	11	12	16	28	40
	25·5	29·9	39·6	68·7	96·1

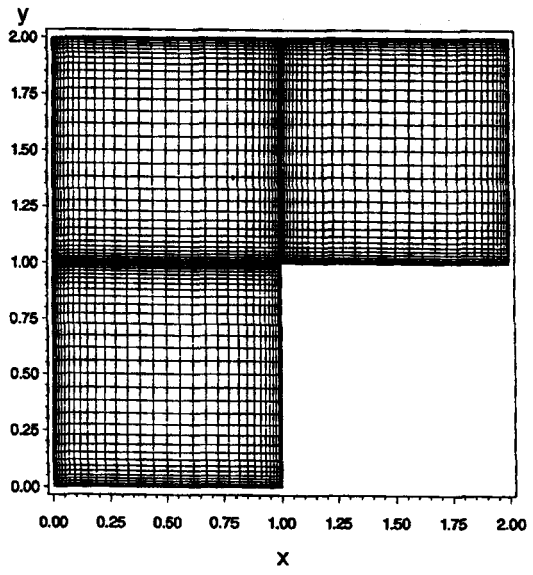

Figure 14. Open cavity stretched grid with AR = 10

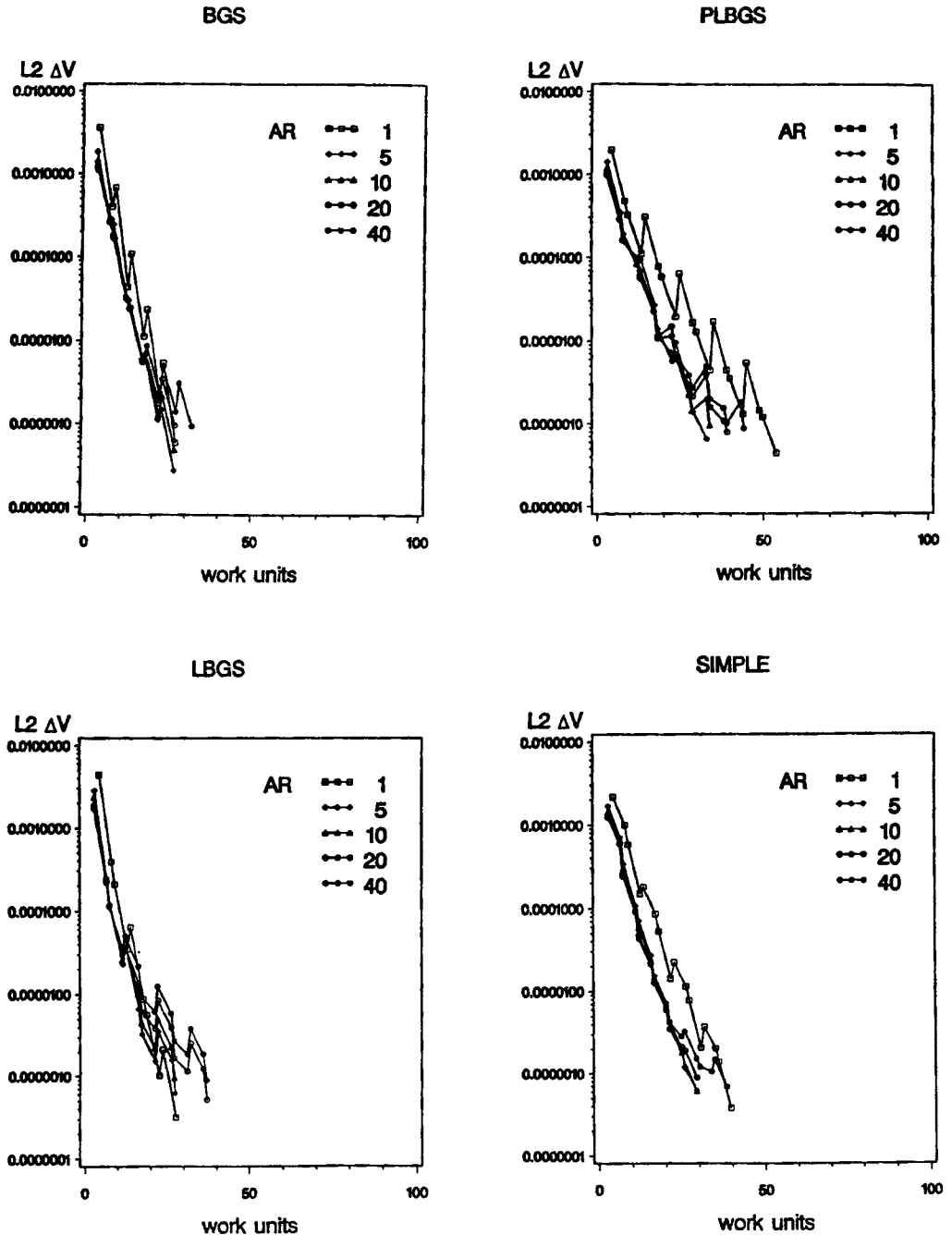

Figure 15. Open cavity convergence histories for all methods on a stretched $128 \times 128 + 256 \times 128$ grid

Table VI. Open cavity convergence on stretched grids for $Re = 1000$

Scheme (r^{fg}_{mom})	AR 1	5	10	20	40
	(cpu seconds/fine-grid sweeps/work units)				
	$64 \times 64 + 128 \times 64$ grid—5 levels				
BGS (0·7)	48·8	40·8	47·3	59·9	67·2
	14	12	14	18	20
	40·2	33·1	38·3	48·8	54·7
PLBGS (0·5)	90·8	46·9	47·2	58·3	79·1
	32	16	16	20	28
	88·1	45·2	45·8	56·1	76·8
LBGS (0·85)	59·0	53·5	52·4	64·7	65·7
	16	15	15	18	19
	43·8	39·1	38·3	47·2	48·1
SIMPLE (0·7)	95·4	64·0	63·7	77·4	91·3
	24	16	16	20	24
	63·0	42·2	41·9	50·8	59·8
	$128 \times 128 + 256 \times 128$ grid — 6 levels				
BGS (0·7)	145·3	143·7	144·9	145·0	173·4
	10	10	10	10	12
	27·1	26·7	26·8	26·9	32·1
PLBGS (0·5)	250·8	153·9	157·0	181·7	206·9
	20	12	13	15	17
	53·9	32·9	33·7	39·0	44·1
LBGS (0·95)	161·5	162·3	161·2	219·5	219·3
	10	11	11	15	15
	27·6	27·4	27·2	37·1	37·0
SIMPLE (0·7)	278·1	208·0	207·6	208·0	272·1
	16	12	12	12	16
	39·7	29·5	29·5	29·5	38·5

7. CONCLUSIONS

From the above results, it is evident that a proper combination of tailored multigrid elements can yield a fast robust solver for the steady incompressible Navier–Stokes equations even on highly stretched grids. In particular, for fine-to-coarse restriction of residuals, the use of full weighting is important on stretched grids. For coarse-to-fine prolongation of corrections, on the other hand, bilinear interpolation works well and is insensitive to the details of the boundary treatment. Finally, a fixed $W(1, 1)$ multigrid cycle appears to offer a good mix of robustness and computational efficiency.

For recirculating flows such as the driven cavity, all four smoothers are effective and competitive. On uniform grids BGS and PLBGS offer a significant advantage over LBGS and SIMPLE, primarily due to less cost per sweep. On stretched grids, BGS and SIMPLE show superior multigrid performance but BGS is substantially cheeper per sweep.

For strongly aligned flows such as that in a developing channel, all four solvers degrade more rapidly with increasing Reynolds number than for recirculating flows with SIMPLE falling off much more rapidly than the others, but they all still converge in under 100 fine-grid sweeps. However, on highly stretched grids, LBGS offers a major advantage in both multigrid performance and net cpu time over the other three smoothers. This is the only case in which an implicit scheme is distinctly superior to the explicit BGS.

For mixed recirculating/aligned flows such as the open cavity, all four smoothers are effective. On uniform grids, SIMPLE again degrades much more rapidly than the others with increasing Reynolds number. On stretched grids BGS offers a small advantage in multigrid performance, but this becomes significant when net cpu time is considered. It is also notable that BGS is less sensitive than the other smoothers to the corner singularity in this flow.

On balance, BGS offers the best mix of robustness and computational speed for all three classes of flows. The semi-implicit schemes PLBGS and SIMPLE offer little or no advantage and, in general, are less robust. The fully implicit LBGS is superior only for the case of highly aligned flows on stretched grids. The pressure correction scheme SIMPLE is, in general, more costly than the other three and degrades much more rapidly than the others with increasing Reynolds number. Finally, since convergence rates using the first-order hybrid scheme are so fast, improving convective differencing from first-order upwind to second-order central by a defect correction procedure similar to that of Thompson and Ferziger[8] should be well worth the extra cost in increased work units for convergence. Also, for a general multigrid solver set up using domain decomposition, it might be highly effective to use BGS over most domains but retain the option to use LBGS in strongly aligned domains.

REFERENCES

1. A. Brandt, 'Multigrid techniques: 1984 guide with applications to fluid dynamics', von Karman Institute, *Lecture Series 1984–04*, 1984.
2. L. Fuchs, 'Multigrid solution of the Navier–Stokes equations on non-uniform grids', in H. Lomax (ed.), *Multigrid Methods*, NASA Conference Publication 2202, Ames Research Center, Moffett Field, CA, 1981, pp. 83–100.
3. L. Fuchs, 'New relaxation methods for incompressible flow problems', in C. Taylor, J. A. Johnson and W. R. Smith (eds), *Numerical Methods in Laminar and Turbulent Flows*, Pineridge Press, Swansea, 1983, pp. 627–640.
4. U. Ghia, K. N. Ghia and C. T. Shin, 'High-*Re* solutions for incompressible flow using the Navier–Stokes equations and a multigrid method', *J. Comput. Phys.*, **48**, 387–411 (1982).
5. S. G. Rubin and P. K. Khosla, 'Navier–Stokes calculations with a coupled strongly implicit method—I', *Comput. Fluids*, **9**, 163–180 (1981).
6. S. P. Vanka 'Block-implicit multigrid solution of the Navier–Stokes equations in primitive variables', *J. Comput. Phys.*, **65**, 138–158 (1986).
7. A. O. Demuren 'Application of multi-grid methods for solving the Navier–Stokes equations', *Proc. Inst. Mech. Engrs., Part C.*, **203**, 255–265 (1989).
8. M. C. Thompson and J. H. Ferziger 'An adaptive multigrid technique for the incompressible Navier–Stokes equations', *J. Comput. Phys.*, **82**, 94–121 (1989).
9. S. Sivaloganathan and G. J. Shaw 'A multigrid method for recirculating flows', *Int. j. numer. methods fluids*, **8**, 417–440 (1988).
10. S. V. Patankar and D. B. Spalding 'A calculation procedure for heat and mass transfer in 3-D parabolic flows', *Int. J. Heat Mass Transfer*, **15**, 1787–1806 (1972).
11. G. J. Shaw and S. Sivaloganathan 'On the smoothing properties of the SIMPLE pressure-correction algorithm', *Int. j. numer. methods fluids*, **8**, 441–461 (1988).
12. E. Dick 'A multigrid method for steady incompressible Navier–Stokes equations based on partial flux splitting', *Int. j. numer. methods fluids*, **9**, 113–120 (1989).
13. D. S. Joshi and S. P. Vanka 'Multigrid calculation procedure for internal flows in complex geometries', *Numer. Heat Transfer, Part B.*, **20**, 61–80 (1991).
14. D. Rayner 'Multigrid flow solutions in complex two-dimensional geometries', *Int. j. numer. methods fluids*, **13**, 507–518 (1991).
15. W. Shyy, M.-H. Chen and C.-S. Sun 'A pressure-based FMG/FAS algorithm for flow at all speeds', 30th Aerospace Sciences Meeting and Exhibit, AIAA 92-0548, (1992).
16. W. A. Mulder 'A new multigrid approach to convection problems', *J. Comput. Phys.*, **83**, 303–323 (1989).